Anodizing of aluminium and AA 2024-T3 alloy in chromic acid: Effects of sulphate on film growth

D. Elabar, G.R. La Monica, M. Santamaria, F. Di Quarto, P. Skeldon, G.E. Thompson

PII: S0257-8972(16)31285-3
DOI: doi: 10.1016/j.surfcoat.2016.11.108
Reference: SCT 21854

To appear in: *Surface & Coatings Technology*

Received date: 10 June 2016
Revised date: 16 November 2016
Accepted date: 29 November 2016

Please cite this article as: D. Elabar, G.R. La Monica, M. Santamaria, F. Di Quarto, P. Skeldon, G.E. Thompson , Anodizing of aluminium and AA 2024-T3 alloy in chromic acid: Effects of sulphate on film growth. The address for the corresponding author was captured as affiliation for all authors. Please check if appropriate. Sct(2016), doi: 10.1016/j.surfcoat.2016.11.108

Anodizing of aluminium and AA 2024-T3 alloy in chromic acid: effects of sulphate on film growth

D. Elabar,[1] G.R. La Monica,[2] M. Santamaria,[2] F. Di Quarto,[2] P. Skeldon[2*], G.E. Thompson[2]

[1]*Corrosion and Protection Group, School of Materials, The University of Manchester, Manchester M13 9PL, U.K.*
[2]*Electrochemical Materials Science Laboratory, Faculty of Engineering, University of Palermo, Viale delle Scienze, 90128 Palermo, Italy*

*corresponding author
E-mail: p.skeldon@manchester.ac.uk
Tel: + 44 161 306 4872

Abstract

Chromic acid anodizing is important for the corrosion protection of aerospace aluminium alloys. Previous study has demonstrated that SO_4^{2-} impurity in the chromic acid affects the film growth on aluminium at a voltage of 100 V. The present work further investigates aluminium and extends the study to industrial anodizing conditions (Bengough-Stuart (B-S) process) and to the AA 2024-T3 alloy. It is shown that SO_4^{2-} concentrations between ~38 – 300 ppm reduce the film growth rate for aluminium anodized at 100 V in comparison with an electrolyte than contains ≤1.5 ppm SO_4^{2-}, whereas ~1500 - 3000 ppm SO_4^{2} have an opposite effect and lead to an unstable pore diameter. Under the B-S process, the film growth depends on the substrate composition, the SO_4^{2-} content of the film, the film morphology and, for the alloy, oxygen generation. Corrosion tests of the alloy in 3.5% NaCl solution revealed better protection with films formed in chromic acid containing 38 ppm SO_4^{2-} compared with ≤1.5 ppm SO_4^{2-}, which are within the specified limits for sulphate impurity for chromic acid anodizing. The difference in corrosion protection is proposed to be related to the observed differences in the film morphologies; it is speculated that this may influence the retention of residues of chromate ions in the films.

Keywords: Aluminium, AA 2024 alloy, anodizing, chromic acid, sulphate

1. Introduction

Anodizing is commonly used to provide protection of aluminium alloys against corrosion and wear [1]. The process generates amorphous alumina films, classically consisting of a thin

barrier region and a thicker porous region with linear pores extending from the barrier region to the film surface [2,3]. However, the presence of intermetallic particles in the alloy and the enrichment of alloying elements at the matrix just beneath the anodic film [4] can lead to modified pores, voids and occluded particles [5-9], and the efficiency of film growth can be reduced significantly by oxygen generation [5]. Furthermore, alloying elements in solid-solution within the alloy matrix can be oxidized and incorporated into the alumina. The concentration of an alloying element species in the film relative to the concentration in the alloy matrix depends upon the migration rate of the species in the barrier region with respect that of Al^{3+} ions [4,5], and also the mechanism of pore formation [6]. For applications that require a high level of corrosion protection, the films are sealed by post-treatments which form precipitates within the pores that block the entry of corrosive species [11-17]. The films may also be employed as a base layer in protection schemes that include an organic primer and topcoat.

Anodizing is usually carried out in chromic, oxalic, phosphoric or sulphuric acid. Chromic acid anodizing is often favoured in coating systems for aircraft, which make use of the effectiveness of corrosion inhibition of aluminium alloys by chromates [18,19]. In industrial processing, sulphate levels in the chromic acid are controlled; for instance, DEFSTAN 03-24/5 specifies a maximum allowable concentration of 0.5 g L^{-1} Na_2SO_4 (≈ 340 ppm SO_4^{2-}) [20]. In recent work, significant effects of SO_4^{2-} at a level of ≈ 38 ppm in anodizing aluminium at 100 V have been reported [21,22]. The SO_4^{2-} reduced the rate of film growth and led to finer pores in the outer part of the film. The present investigation examines the effect of a wider range of sulphate concentrations, anodizing of the high strength AA 2024-T3 alloy, and use of the (Bengough-Stuart) B-S process, which employs stepping the voltage, that is commonly employed in industry.

2. Experimental

The materials comprised 99.99 % aluminium and AA 2024 alloy sheets of 0.3 and 1 mm thickness, respectively. The alloy was in the T3 condition, i.e. solution-treated, cold worked and naturally aged. The nominal composition of the alloy in wt.% is 3.8-4.9% Cu, 1.2-1.8% Mg, 0.3-0.9% Mn, 0.5% max. Si, 0.5% max. Fe, 0.25% max. Zn, 0.15% max. Ti, 0.1% max. Cr, 0.15% other elements, bal. Al. The AA 2024-T3 alloy typically contains Al_2CuMg, Al_2Cu and Al-Cu-Fe-Mn-(Si) intermetallic particles, of size in the range 0.1- 10 µm, rod-shaped Al-Cu-Mn dispersoids with lengths of a few hundred nanometres, and Al_2Cu grain boundary precipitates [23-27]. Specimens of dimensions 3.0 x 1.5 cm were cut from the sheets. The aluminium specimens were then electropolished at 20 V for 3 min in 60% perchloric acid/ethanol (20/80 by vol.) at 278 K, followed by rinsing in ethanol and then deionized water, and drying in a cool air stream. The alloy specimens were etched for 60 s in10 wt % NaOH at 333 K, de-smutted in 30 vol % nitric acid at room temperature for 30 s, rinsed in deionized water and dried in a cool air stream.

The pre-treated specimens were then masked with lacquer (Stopper 45 MacDermid), leaving a working area of ~3 cm^2 on one side, and anodized in a two-electrode cell containing 500 cm^3 of 0.4 M chromic acid at 313 ± 1 K. The electrolyte was stirred during anodizing using a magnetic stirrer. The chromic acid was prepared using deionized water and two sources of chromic oxide, which resulted in electrolytes containing ≤1.5 and 38 ppm SO_4^{2-}, designated low and high sulphate chromic acid (LSCA and HSCA), respectively. The details of the electrolytes have been given previously [21]. Electrolytes containing up to 3000 ppm SO_4^{2-} were also prepared using LSCA with additions of either H_2SO_4 or Na_2SO_4 (95-98% and 99%

purity, respectively). Each specimen was connected to an insulated aluminium rod and held vertically in the centre of the cell. The cathode was a cylindrical aluminium sheet, with an area of ~210 cm^2, which was separated from the specimen by a distance of ~5 cm. The electrolyte temperature was controlled using a heater/stirrer unit with a contact thermometer (C-MAG HS 7 digital IKAMAG/ETS-D5). Anodizing employed a Goodwill Instruments Co. GPR-100H05 power supply, with the current recorded every 0.1 s by a computer with Labview software. Anodizing was carried out either at a constant voltage of 100 V for 600 s or using the B-S process. The latter involved increasing the voltage in steps up to 50 V; the specimens anodized in LSCA and HSCA used the following voltage sequence: 10 V steps up to 30 V, and then 5 V steps up to 40 V, with each step lasting for approximately 150 s; the voltage was then held at 40 V for 20 min, then increased in 2 V steps up to 48 V, with each step lasting for approximately 60 s. The voltage was maintained at 48 V for 120 s, then increased to 50 V and held at this value for 5 min. The voltage steps in the period of anodizing up to 40 V for specimens anodized in electrolytes containing 1500 ppm SO_4^{2-} were slightly different to the previous values: 8 V steps were used up to 32 V and then 4 V steps up to 40 V, with each step lasting for approximately 120 s. The anodizing procedure after reaching 40 V followed that previously described for the other specimens. Following anodizing, the specimens were rinsed in de-ionized water and dried in a cool air stream.

In addition to the studies using bulk aluminium specimens, an aluminium layer and an underlying nanolayer of Al-W alloy were deposited by magnetron sputtering on electropolished aluminium substrates, according to the previously described procedure [6]. The specimens were then anodized at 100 V in chromic acid containing ~900 ppm SO_4^{2-} at 313 K; anodizing was terminated when the tungsten nanolayer was incorporated into the barrier region of the porous film. The Al-W layer was used for examination of the effect of

the SO_4^{2-} on the mechanism of pore formation. For the bulk specimens of aluminium and aluminium alloy, and also for the sputtering-deposited aluminium, the current-time responses were checked for reproducibility in duplicated or triplicated experiments.

Cross-sections of anodized specimens were examined by scanning electron microscopy (SEM) using a Zeiss Ultra 55 instrument, operated at 1.5 kV. The cross-sections were prepared on a Leica Ultracut UCT ultramicrotome using a diamond knife. Specimens were also examined following dissolution of the anodic film in a mixture of 20 g l^{-1} of CrO_3 and 35 ml l^{-1} H_3PO_4 for 10 min at 333 K, which reveals replicas of the cell bases in the aluminium and alloy substrates.

The sputtering-deposited specimens were examined by transmission electron microscopy in a Philips CM 20 instrument, operated at 200 kV. Sections, nominally 15 nm thick, were obtained using a Leica Ultracut UCT ultramicrotome with a diamond knife.

The corrosion resistance of the anodized AA 2024-T3 alloy was assessed using specimens anodized by the B-S process in LSCA and HSCA that were immersed in naturally-aerated 3.5% NaCl solution at room temperature for times of up to 15 days. After immersion, the specimens were rinsed in deionized water, dried in a cool air and examined by optical microscopy and SEM.

3. Results

3.1. Anodizing aluminium at 100 V

Figures 1 (a,b) show the current density-time curves for aluminium anodized at 100 V for 600 s in electrolytes containing 150 to 3000 ppm SO_4^{2-}, added as H_2SO_4 and Na_2SO_4, respectively, and also in LSCA (≤ 1.5 ppm SO_4^{2-}) and HSCA (38 ppm SO_4^{2-}). Since the SO_4^{2-} sources had similar effects, later experiments used only Na_2SO_4 to add SO_4^{2-}. The current densities for SO_4^{2-} contents up to 900 ppm first decreased then rose to a steady value due to the initial formation of a barrier layer, the development of pores and the final porous film growth. At SO_4^{2-} concentrations of 38 to 900 ppm, the steady current density was reduced by up to a factor of ≈ 2 relative to anodizing in electrolytes containing either ≤1.5 or 1500 ppm SO_4^{2-}. With 1500 ppm SO_4^{2-}, several peaks of diminishing height preceded the steady current region. One peak is observable in the current density-time curve for anodizing in the electrolyte containing 900 ppm SO_4^{2-} added as H_2SO_4 (Fig. 1 (a)), and a low second peak is discernible when the addition was made as Na_2SO_4 (Fig. 1 (b)). The presence of the second peak was not dependent on the method of SO_4^{2-} addition, since the peak could also be sometimes observed with addition of H_2SO_4. At 3000 ppm SO_4^{2-}, the peaks were superimposed on a rising current. The latter suggests a transition in the anodizing behaviour; in this regard, the current density at a given voltage is higher for sulphuric acid anodizing than for chromic acid anodizing [28].

Since previous work has presented the morphologies of the films formed on aluminium at 100 V in electrolytes containing low levels of SO_4^{2-} [21,22], the present investigation focused on the higher SO_4^{2-} concentrations. Figure 2 (a) presents scanning electron micrographs of a cross-section of a film formed for 600 s in an electrolyte containing 3000 ppm SO_4^{2-}. The film thickness ranged from 1737 to 2058 nm; the average thickness was 1942 nm, which corresponds to a growth rate of ~3.2 nm s^{-1}. The anodizing charge density passed in forming the film, which was determined from integration of the current-time curve, was ~5.450 C cm^{-}

^{2}; this charge density could oxidize 1884 nm of aluminium, assuming that the charge is used only to form Al^{3+} ions. Hence, the ratio of the thicknesses of the film and oxidized aluminium is ~1.03, which is a typical value for chromic acid anodizing [21,22]. Pores are orientated approximately normal to the film surface and the film base is uniformly scalloped, which contrasts with the less regular film morphologies formed in LSCA or HSCA [22]. The pores also lack the feathering typical of chromic acid anodizing [29]. Figure 2 (b) shows a region where the film had fractured during cutting with the diamond knife. About 10 to 15 relatively major changes of diameter occur in the individual pores (see arrows). Rib-like rings sometimes occur between the narrow regions. The anodizing time and the number of diameter changes suggest that the major changes in diameter occur at intervals of roughly 50 s, which is similar to the intervals between the peaks in the current density-time curve that occurred during anodizing the specimen (Fig. 1). The decrease in the height of the peaks as the anodizing proceeds is possibly due to the diameter changes in different pores becoming progressively out of phase. The barrier layer thickness, measured at a pore centre, was ~85 nm, compared with ~100 nm for films formed in LSCA and HSCA [21,22]. Point EDX analyses across the film thickness (Table 1) showed a decrease in the atomic ratio of S:Al from ~0.05 at the film surface to ~0.02 at the film base. The former ratio is similar to that reported in films formed in electrolytes containing about 0.4 M sulphuric acid at current densities in the range ~1 to 3 mA cm^{-2} [30-32]. In the electrolyte containing 3000 ppm SO_4^{2-} (3.1×10^{-2} M) , the SO_4^{2-} concentration is approximately 13 times lower than the concentration of Cr(VI) species. The similarity of the S:Al ratios in the surface region of present film and films formed in sulphuric acid suggests that SO_4^{2-} ions are adsorbed preferentially to Cr(VI) ions at the pore bases.

Figure 3 shows transmission electron micrographs of sputtering-deposited aluminium specimens before (Fig. 3 (a)) and after (Figs. 3 (b,c)) anodizing at 100 V with 900 ppm SO_4^{2-}. (Higher concentrations of SO_4^{2-} caused blistering of the deposited layer, suggesting that a high compressive stress was generated in the film.) The sputtering-deposited layer reveals columnar grains of aluminium. The thin, dark band at the base of the layer (see arrow in Fig. 3 (a)) contains the tungsten tracer. The electropolished aluminium is located beneath the tungsten-containing band. Anodizing of the specimen was stopped when the oxidized tungsten resided in the barrier layer, which was indicated by a fall in the current density [22]. The tungsten layer remained relatively flat as it crossed the barrier layer and was incorporated into the pore walls; the presence of the tungsten in the pore walls is evident at the right-hand side of the micrograph shown in Fig. 3 (b). The morphology of tungsten layer contrasts with that in films formed in electrolytes such as phosphoric acid where flow of the alumina in the barrier layer causes a distortion of the tracer band into a U-shape and prevents the W^{6+} ions reaching the pore bases [6,33]. The behaviour of the tungsten during anodizing in the present film is similar to that reported previously for anodizing in chromic acid with no addition of SO_4^{2-} [22]. Evidently, the addition of 900 ppm SO_4^{2-} did not alter the mechanism of pore formation significantly, which is also suggested by the current-density-time curves (Fig. 1), since only at 3000 ppm SO_4^{2-} was a major change observed in the shape of the curves. W^{6+} ions migrate in anodic alumina at ~0.3 times the rate of Al^{3+} ions [34]. Hence, the tungsten approximates to a marker. A comparison of the depth of the tungsten layer in the specimens before and after anodizing shows that the film is ~1.16 times thicker than the oxidized aluminium, which is within the range of values expected for films formed in chromic acid [22].

3.2. Anodizing aluminium and AA 2024-T3 alloy using the B-S process

Figure 4 (a) presents the current density-time curves for aluminium anodized by the B-S process using electrolytes containing ≤1.5 (LSCA), 38 (HSCA) or 1500 ppm SO_4^{2-}. The last concentration is near the upper limit for maintaining a constant rate of porous film growth, as evident from the current-time curves of Fig. 1. Spikes in the current density that occur after each voltage step are mainly due to the rapid thickening of the barrier layer that immediately follows each step increase in the electric field. The increments in the current density tend to reduce with subsequent steps as the percentage change in the voltage decreases. A much higher current density (~8.8 mA cm^{-2}) is achieved in the period of anodizing at 40 V in the electrolyte containing 1500 ppm SO_4^{2-} than with anodizing in the electrolytes containing ≤1.5 or 38 ppm SO_4^{2-} (~ 3.6 mA cm^{-2}).The latter value compares with ~4.5 and 2.8 mA cm^{-2} for anodizing at 100 V electrolyte containing ≤1.5 and 38 ppm SO_4^{2-}, respectively. An increase in the current density is normally expected with an increase in voltage, which is contrary to the reduced current density for aluminium anodized at 100 V in the electrolyte containing 38 ppm SO_4^{2-} (HSCA) relative to anodizing at 40 V in the same electrolyte using the B-S process. This may be due to the differing morphologies of the films formed at constant voltage and with a stepped voltage that influences the composition of the electrolyte in the pores, as discussed later.

Figures 5 (a-c) shows scanning electron micrographs of cross-sections of the films formed on aluminium, using the B-S process, in electrolytes containing ≤1.5, 38 and 1500 ppm SO_4^{2-}, revealing thicknesses of ~3130, 3320 and 7200 nm, respectively, which indicate average growth rates of 1.30, 1.38 and 3.00 nm s^{-1}. The respective anodizing charge densities of 8.839, 8.470 and 19.164 C cm^{-2} can oxidize 3055, 2927 and 6624 nm of aluminium. Hence, the ratios of the film thickness to oxidized aluminium thickness are ~1.02, 1.13 and 1.09,

respectively. The cell and pore diameters increase between the film surface and the substrate due to the increases in voltage during the anodizing process. Contrasting with the film formed in the electrolyte containing ≤1.5 ppm SO_4^{2-} (Fig. 5 (a)), the pores in the film formed in the electrolyte containing 38 ppm SO_4^{2-} diverged significantly from an orientation generally normal to the film surface at depths beyond ~1000 nm, resulting in a cusped aluminium/film interface (Fig. 5 (b)). A similar change in the pore orientation was reported in an earlier study during anodizing of aluminium in HSCA at 100 V, when clusters of larger cells developed at the film base as the SO_4^{2-} incorporation into the film reduced with increasing thickness of the film [22]. The charge density required for forming the outer 1000 nm of the film thickness, which was determined using Faraday's Law and the previous film/oxidized aluminium thickness ratio of 1.13, is 2.560 C cm^{-2}. This charge density is passed following anodizing for 915 s, which is shortly after the voltage step to 40 V is completed. EDX analyses of the film formed by the B-S process in HSCA (Table 1) showed that the S:Al atomic ratio reduced from ~0.012 at the film surface to negligible levels at depths of >2000 nm. The film formed on aluminium by the B-S process in the electrolyte containing 1500 ppm SO_4^{2-} displays linear pores (Fig. 5 (c)), which are shown at higher magnification in Fig. 5 (d). The pore walls reveal ribs separated by distances of roughly 30 to 60 nm, accompanied by striations in the fractured cell walls. The rib separation is much less than for the specimen anodized at 100 V using 3000 ppm SO_4^{2-}. However, unlike the latter specimen, no peaks were resolved in the current density-time curve of Fig. 4(a), possibly because the pore diameter changes are smaller, more frequent, and obscured by variations in the current density caused by the voltage steps.

Figure 4 (b) shows the current density-time curve for the AA 2024-T3 alloy anodized in electrolytes containing ≤1.5 (LSCA), 38 (HSCA) or 1500 ppm SO_4^{2-}. Opposite to the increase

in the current density observed with aluminium, the presence of 38 and 1500 ppm SO_4^{2-} in the electrolyte mainly caused the current density to decrease by ~40 and 30%, respectively. Figures 6 (a,-c) show scanning electron micrographs of cross sections of the anodized AA 2024-T3 specimens revealing average film thicknesses of 3523±152, 2381±91 and 3246±134 nm following anodizing in electrolytes containing ≤1.5 (LSCA), 38 (HSCA) or 1500 ppm SO_4^{2-}, respectively, corresponding to average growth rates of 1.47, 0.99 and 1.35 nm s^{-1}. The backscattered electron images disclose second phase particles in the alloy and the films as bright features. The film surfaces are flat compared with the film bases, which are very irregular and cause the local film thickness to vary by up to 15% about the average values. Darker regions occur where the film had fractured during cutting. In the latter regions, the films appear to comprise layers of cell bases and lateral porosity, contrasting with the linear porosity of films on aluminium. This type of film morphology has been also found on the AA 2024-T3 alloy following anodizing in sulphuric acid [5]. From the charge densities passed of 16.09, 11.30 and 12.79 C cm^{-2} for anodizing in electrolytes containing ≤1.5, 38 or 1500 ppm SO_4^{2-}, respectively, which can oxidize 5562, 3906 and 4421 nm of aluminium, the ratios of the film thickness to the oxidized aluminium thickness are 0.63, 0.61 and 0.73, respectively. These are lower than for anodizing aluminium due to oxygen generation during anodizing that occurs at locations of intermetallic particles and above the copper-enriched alloy matrix. According to EDX point analyses, the S:Al atomic ratio in the film formed with 1500 ppm SO_4^{2-} (Table 1) ranged from ~0.02 to 0.04, with no clear relationship to the depth within the film.

Figures 7 (a,b) show scanning electron micrographs of the aluminium following chemical stripping of films formed to 50 V (i.e. at the end of the B-S anodizing process) in LSCA (≤ 1.5 ppm SO_4^{2-}) and HSCA (38 ppm SO_4^{2-}), respectively. The cell replicas in the substrate are

distributed across a relatively flat substrate surface following removal of the film formed in LSCA, whereas cells are distributed within deep scallops, of ~1 to 3 μm diameter, in the surface originally anodized in HSCA; the scallops correspond to the cusped aluminium/film interface shown in the scanning electron micrograph of Fig. 5(b). The cell diameter ranged from about 10 to 280 nm, with an average of ≈160 nm. The scallops were absent for substrates anodized in HSCA to 16 and 32 V (not shown). The divergence of the pores that occurs at a depth of about 1000 nm in the film thickness, noted earlier in the cross-section of the film formed in HSCA shown in Fig. 5 (b), suggests that the scallops form during anodizing at 40 V. Following stripping of films formed by the B-S process to 50 V on the alloy in LSCA (≤ 1.5 ppm SO_4^{2-}) and HSCA (38 ppm SO_4^{2-}), a much rougher surface than for the aluminium was revealed (Figs. 7 (c,d), respectively), with some cell replicas being contained in deep cavities of similar size to the roughness variations in the film cross-section of Fig. 6(a,b); the cavities are smaller with HSCA than with LSCA. The roughness of the surfaces made it difficult to measure the cell sizes reliably.

Table 2 lists the total charge densities passed during anodizing the various specimens of the present study. The results are given as the average and standard deviation of three or four repeated experiments, except for 1500 ppm SO_4^{2-} when two specimens were anodized. The results demonstrate the significant differences in the anodizing behaviours that are caused by the different levels of SO_4^{2-}, which are dependent upon the particular anodizing condition employed and the composition of the substrate.

3.3. Corrosion tests of anodized AA 2024-T3 alloy

Figures 8 (a,b) show optical microscopy images of the AA 2024-T3 alloy anodized in LSCA ($\leq$ 1.5 ppm SO_4^{2-}) and HSCA (38 ppm SO_4^{2-}) using the B-S process and then immersed for 15 days in 3.5% NaCl solution. A large difference is evident between the appearances of the specimens. The LSCA specimen exhibited relatively numerous locations where the film was degraded and the substrate was exposed. These sites had diameters of up to 300 µm. Such sites were absent on specimens that had been immersed for 7 days and then examined by optical microscopy. In contrast, after 15 days immersion in 3.5% NaCl solution, the film on the HSCA specimen was less degraded and the substrate was not exposed. Figures 8(c,d) present scanning electron micrographs of the surfaces, revealing cracked and detached film in the localized regions of degradation on the LSCA specimen. The film was less damaged on the HSCA specimen and the substrate was not exposed by loss of the film. Examination of a cross-section prepared by ultramicrotomy at a region of the LSCA specimen where the substrate had been exposed showed that the corrosion of the alloy had occurred to a depth of roughly 50 µm (Fig. 8(e)). In contrast, a cross-section of the HSCA specimen revealed that the localized attack by the solution was confined to the film (Fig. 8(f)). The observations of a superior corrosion protection by the film formed in the electrolyte containing 38 ppm SO_4^{2-} were confirmed in a duplicated experiment using the same test conditions. The degradation of the film and the alloy possibly occurs at the locations of intermetallic particles. The oxidation of the particles can create defects in the anodic film, such as voids, and generate localized regions of the film with modified compositions and morphologies. At these regions, Cl^- ions have easier access to the alloy and may initiate pitting and intergranular corrosion. Intermetallic particles that have not been fully oxidized may also provide local cathodes for reduction of oxygen that enhance the corrosion rate. However, the corrosion of the alloy may be inhibited by residual chromate ions in the film [35] that diffuse to regions of exposed alloy, where they are either adsorbed on the alloy surface to displace adsorbed Cl^- ions or

reduced at cathodic sites to form a Cr(III) oxide/hydroxide film [18,19]. Furthermore, the porosity in the film that allows access of Cl^- ions to the alloy surface may be blocked by hydration of the alumina. Thus, the better corrosion protection of the alloy by anodizing in HSCA compared with anodizing in LSCA may be due to a greater amount of residual chromate ions in the film and easier blocking of pores, for instance due to a finer size of pores near the film surface.

4. Discussion

4.1. Effect of the film morphology on SO_4^{2-} incorporation into films formed an aluminium

In the authors' earlier study of aluminium anodized at 100 V, the steady current density was reduced during the early period of anodizing in HSCA relative to the same period of anodizing in LSCA. After this period, the current density slowly rose and became similar to that for anodizing in LSCA after a time of about 2000 s. The rise was attributed to the SO_4^{2-} depletion, which was measured by EDX analysis, in the barrier region of the film; the depletion occurs as the rate of SO_4^{2-} diffusion down the pores slows as the film thickens and the pores lengthen [22]. The effect of the film thickening on the supply of SO_4^{2-} is also evident in the reducing S:Al ratio with film depth measured by EDX spectroscopy (Table 1) for the aluminium specimen anodized for 600 s at a constant voltage of 100 V in the electrolyte containing 3000 ppm of SO_4^{2-}(Fig. 2).

Anodizing of aluminium in HSCA using the B-S process resulted in a reduced current density relative to LSCA only during the sequence of voltage steps up to 40 V (Fig. 4 (a)). Since the pore population density in anodic films is usually proportional to V^{-2}, the population density

at the film base during anodizing using the B-S process is expected to be reduced by factors of 16 and 25 between the first voltage step to 10 V and those to 40 V and 50 V, respectively. The factors may be underestimated if the formation ratio for cells at the start of film growth is reduced compared to later stages due to the greater amount of SO_4^{2-} incorporated to the film near the start of anodizing, as observed in previous work for aluminium anodized in HSCA at 100 V [22]. Thus, in the films formed under the voltage steps of the B-S process, most surface pores are terminated within the main body of the film and only a small proportion provide a pathway for ions to diffuse between the film surface and the barrier layer. Hence, the supply of SO_4^{2-} from the bulk electrolyte to the film base and the diffusion of Al^{3+} ions, which are ejected from the film to the pore electrolyte, from the barrier layer to the film surface are restricted compared with films formed at constant potential. The more rapid changes in the composition of the electrolyte at the pore bases brought about by the restricted diffusion of SO_4^{2-} and Al^{3+} ions during anodizing of aluminium in LSCA and HSCA using the B-S process may explain the achievement of similar current densities after only about 600 s (Fig. 4 (a)) in comparison with a requirement for anodizing for a much longer time of about 2500 s at constant voltage of 100 V ([22]). It may also explain the reduced current density for anodizing aluminium at 100 V (Fig. 1) compared with the lower voltage of the B-S process (Fig. 4 (a)), noted earlier, for an electrolyte containing 38 ppm SO_4^{2-}, since under the latter condition supply of SO_4^{2-} ions to the barrier layer is restricted by the modified film morphology.

4.2. Effect of SO_4^{2-} incorporation on the pore diameter in films formed on aluminium

Other work has shown that the incorporation of SO_4^{2-} ions into porous films formed on aluminium in sulphuric acid increases linearly with the logarithm of the current density,

suggesting a dependence of the incorporation on the electric field [30-32]. Therefore, the depletion of SO_4^{2-} with increasing depth in the film formed on aluminium in the present work at 100 V in the chromic acid electrolyte containing 3000 ppm SO_4^{2-} (Table 1), owing to the slowing of the diffusion of SO_4^{2-} ions in the pores to the barrier layer, may be mitigated to some degree by the increase in the current density that occurs as the film grows. It is suggested that the variable pore diameters that were observed in films formed by anodizing aluminium in electrolytes containing 1500 and 3000 ppm SO_4^{2-} under the stepped potential of the B-S process or under a constant potential of 100 V, respectively (Figs. 5 (d) and 2 (b)), is related to variations in the SO_4^{2-} concentration in the barrier layer due to influences of diffusion on the composition of the electrolyte at the pore bases, and hence on the adsorption of chromate and SO_4^{2-} ions at the barrier layer surface and the subsequent incorporation of the latter ions into the film. A fluctuating composition of the outer region of the barrier layer due to the periodic enrichment and depletion of incorporated SO_4^{2-} ions could then affect a range of factors that determine the rate of film growth and the formation of the porous film morphology. Studies of barrier-type films formed on aluminium have identified a retained charge in a thin layer at the film surface, which was suggested to be due anion species incorporated into the film surface [36]; the retained charge, and the equal but opposite charge at the aluminium/film interface, resulted in an electric field that remained across the film when anodizing was terminated. Thus, variations in the concentrations of SO_4^{2-} ions in the present films may affect the magnitude of the charge and the electric field in the film during film growth. Furthermore, studies of the stress distribution in barrier films formed in phosphoric acid have identified the presence of a high compressive stress in a thin layer of the film adjacent to the film surface; the layer contained an enhanced concentration of incorporated phosphate species and the stress was suggested to cause to flow of the film material. Therefore, a variable rate of incorporation of SO_4^{2-} ions into barrier layer at the base

of the pores of the present films may lead to a variable stress in the film, which could affect the flow of the oxide. The incorporation of SO_4^{2-} ions may also affect the ionic transport across the film, which occurs by a high-field migration process; the kinetics of the process can be described by the relationship [38]:

$J = A \exp-(Q-qaE)/kT$

in which J is the ionic current density, A is a constant at a given temperature, Q is an activation energy for diffusion of the mobile defect, q is the charge of the defect, a is the distance of migration required to overcome the activation energy barrier, k is the Boltzmann constant, T is the temperature. Thus, incorporated SO_4^{2-} ions may affect the current density through their influence on the space charge in the film and the structure of the film that affect Q, a and E. DeWit and Thornton have recently presented a theoretical analysis of film growth that links the ionic transport in the bulk film and the reactions occurring at the film surface [39]. The model indicates that changes in the potential distribution at the film surface due to the variable incorporation SO_4^{2-} ions could affect the rate of ejection of Al^{3+} ions from the film surface to the electrolyte. Finally, it is well known that the atomic arrangement in the amorphous structure of anodic alumina is dependent upon the conditions of film formation [40-43]. Amorphous anodic films formed on aluminium usually consist of a mixture of 4-, 5- and 6-fold co-ordination of Al^{3+} ions with O^{2-} ions, whereas films formed in chromic acid display only 6-fold co-ordination [43]. Hence, variable rates of incorporation of SO_4^{2-} ions could cause variations of the co-ordination of Al^{3+} ions within the film that could lead to differing local values of the activation energy and jump distance.

The change in the pore diameter during the growth of the film may be caused by the effect of the varying electrolyte composition and film composition at the pore bases on either field-assisted dissolution or flow of the alumina, or a combination of the two processes. For

instance, the oxide flow may be promoted by a transient increase in the incorporation of SO_4^{2-} ions, which causes a localized compressive stress that is relieved by oxide displacement. The stress could arise due to the relatively large molar volume of $Al_2(SO_4)_3$, which is about 3.9 times that of amorphous Al_2O_3. Since the diameter changes that occur in adjacent cells are not in phase, the outward displacement of oxide in a particular cell may be constrained by adjacent cells. Oxide may then flow into the pore volume to reduce the pore diameter, as has been observed to occur by other investigators under conditions where the flow of the oxide is constrained [44]. Notably, the current density during anodizing in the electrolytes containing 1500 and 3000 ppm SO_4^{2-} is significantly above the threshold of 3 mA cm^{-2}, at which stresses were observed to change from tensile to compressive in films formed on aluminium in phosphoric acid [45]. However, since films formed in high purity chromic acid contain a negligible amount of incorporated anions, unlike the films formed in phosphoric acid, the stress in the film may remain tensile to higher current densities compared with anodizing in phosphoric acid. The presence of the tensile stress may explain the feathering of the pore walls that occurs in films formed in electrolytes containing low concentrations of SO_4^{2-}, which may be generated by formation of cracks in the region of the barrier layer.

4.3. Effect of substrate composition

Unlike aluminium, when the alloy is anodized by the B-S process, the current density during anodizing in HSCA (38 ppm SO_4^{2-}) remains about 40% lower than that in LSCA ($\leq$ 1.5 ppm SO_4^{2-} at all times during the process (Fig. 4 (b)). The anodizing of the alloy is more complicated compared with anodizing of aluminium due to the differences in the composition and morphology of the film and the generation of oxygen during the film growth. Oxygen can be generated at locations of intermetallic particles and also above the matrix, where it is

associated with enrichment of alloying elements beneath the anodic film [5]. Alloying element species in solid solution in the matrix, i.e. copper, magnesium, manganese and iron, are oxidized and incorporated into the amorphous alumina structure, and copper, iron and manganese are enriched in the alloy [46-49]. The enrichment of the present alloy is established during the alkaline etching [50], and hence the alloying element species are incorporated into the anodic film above the matrix from the start of anodizing. Copper, magnesium, manganese and iron species migrate outward in the barrier layer faster than the Al^{3+} ions [5, 47-49,51], and are lost to the electrolyte at the pore base. The incorporation of alloying element species in the anodic alumina may affect the ionic resistivity of the film and hence be a factor in explaining differences in the current density between anodizing the alloy and aluminium during anodizing at a particular voltage.

4.4. Effect of oxygen generation in anodizing the AA 2024-T3 alloy

It is well known that oxygen generation accompanies the film growth on AA 2024-T3 alloy [5]. The migration of Al^{3+} and O^{2-} ions in the film account for ~40 and 60% of the ionic current in a barrier-type or porous film formed on high purity aluminium [52,53]. A similar contribution of cation migration to the ionic current is expected for the alloy. For the film formed on aluminium by the B-S process, a current efficiency of about 60% is expected, since oxygen evolution under this condition of film growth is negligible and the only contribution to the loss in current efficiency is due to the ejection of Al^{3+} ions to the electrolyte that migrate across the barrier layer to the pore bases. Under this condition, an average value of ~1.08 was obtained for the ratios of the film thickness, measured from scanning electron micrographs of film cross-sections, and the thickness of oxidized aluminium, calculated from the charge passed in the cell during anodizing, for anodizing of

aluminium under the B-S process in electrolytes containing ≤ 1.5, 38 and 1500 ppm SO_4^{2-}. In contrast, an average ratio of 0.66 was determined for the alloy. It is reasonable to assume that a similar thickness of oxide was formed from oxidation of a given thickness of either the aluminium substrate or the alloy substrate, since the films are mainly composed of anodic alumina in both instances. Furthermore, the proportions of the ionic current in the barrier layer carried by Al^{3+} and O^{2-} ions are expected to be similar in the films formed on aluminium and the alloy, since the barrier layer contains only low concentrations of alloying element species. Hence, the amount of the charge passed in the cell that is used to form oxygen gas can be roughly estimated from the difference in the thickness of ratios for anodizing the aluminium and the alloy, i.e (1.08-0.66)/1.08. This suggests that roughly 40% of the charge passed through the cell during anodizing the alloy was consumed by generation of oxygen. Some of the gas may be trapped in bubbles at high pressure within the alumina, the remainder is evolved from the film surface. The evolution of the gas may displace the electrolyte from pores, allowing its subsequent replacement by fresh electrolyte. This replenishment may explain the absence of a dependence on film depth of the S:Al ratio measured by EDX analysis (Table 1), since a fresh supply of SO_4^{2-} ions to the pore bases is provided by the ingress of electrolyte of the bulk composition.

5. Conclusions

1. Anodizing of aluminium and AA 2024-T3 alloy under voltage control in chromic acid at 313 K is sensitive to the concentration of SO_4^{2-} impurity in the electrolyte, which can affect the rate of film growth and the film morphology, even at SO_4^{2-} levels within normally specified limits for chromic acid anodizing. The differences in the behaviours between the various anodizing conditions and substrate compositions investigated in the study are related

to the differences in the film morphology, the sulphur content of the films and, for the alloy, the evolution of oxygen.

2. Sulphate concentrations in the range 38-300 ppm reduce the current density during anodizing of aluminium at 100 V in comparison with electrolytes containing either $\leq$ 1.5 or $\geq$ 1500 ppm SO_4^{2}. The current density is greatly increased by anodizing in electrolytes containing 3000 ppm $SO_4^{2-}$and oscillations in the current density are associated with a periodic variation in the cell wall thickness and the pore diameter. The behaviour of a tungsten nanolayer tracer during anodizing of sputtering-deposited aluminium at 100 V in an electrolyte containing 900 ppm SO_4^{2-} indicates that the mechanism of the coating growth was not substantially altered by SO_4^{2-} concentrations up to this level.

3. The current density and the film thickness are significantly reduced for the AA 2024-T3 alloy anodized using the B-S process in an electrolyte containing 38 ppm SO_4^{2-} compared with an electrolyte containing <1.5 ppm SO_4^{2-}. Furthermore, contrasting with anodizing of aluminium, anodizing of the alloy leads mainly to a reduction in the current density by anodizing in an electrolyte containing 1500 ppm SO_4^{2-}. The stepped voltage employed in the B-S process results in restricted transport of ionic species between the film surface and the barrier layer, which affects the composition and growth rate of the film.

4. Anodizing of the AA2024-T3 alloy in chromic acid containing 38 ppm SO_4^{2-} resulted in better corrosion protection of the alloy in comparison with anodizing in chromic acid containing <1.5 ppm SO_4^{2-} following immersion in 3.5 wt.% NaCl for 15 days. The better corrosion protection is suggested to be due to the more favourable morphology of the film.

Acknowledgements

The authors thank the Engineering and Physical Sciences Research Council (LATEST 2 Programme Grant, EP/H020047/1) for support of this work. They are also grateful to the support of the University of Palermo and for the award of a Scholarship from the EU Erasmus Programme to G.R. La Monica.

References

[1] P.G. Sheasby and R, Pinner, The Surface Treatment and Finishing of Aluminium and its Alloys, 6th Edition, Finishing Publications Limited and ASM International, 2001, vol. 1, 427-535.

[2] F. Keller, M.S. Hunter, D.L. Robinson, Structural features of oxide coatings on aluminium, J. Electrochem. Soc. 100 (1953) 411-419.

[3] J.P. O'Sullivan, G.C. Wood, The morphology and mechanism of formation of porous anodic films on aluminium, Proc. R. Soc. London, Ser. A 317 (1970) 511-543.

[4] H. Habazaki, K. Shimizu, P. Skeldon, G.E. Thompson, G.C. Wood, X. Zhou, Effects of alloying elements in anodizing of aluminium alloys, Trans. Inst. Met. Finishing 75 (1997) 18-23.

[5] L. Iglesias-Rubianes, S.J. Garcia-Vergara, P. Skeldon, G.E. Thompson, J. Ferguson and M. Benecke, Cyclic oxidation processes during anodizing of Al-Cu alloys, Electrochim. Acta 52 (2007) 7148-7157.

[6] S.J. Garcia-Vergara, P. Skeldon, G.E. Thompson, H. Habazaki, A flow model of porous anodic film growth on aluminium, Electrochim. Acta 52 (2006) 681-687.

[7] L.E. Fratila-Apachitei, F.D. Tichelaar, G.E. Thompson, H. Terryn, P. Skeldon, J. Duszczyk, L. Katgerman, A transmission electron microscopy study of hard anodic oxide layers on AlSi(Cu) alloys, Electrochim. Acta 49 (2004) 3169–3177.

[8] Y. Ma, X. Zhou, G.E. Thompson, M. Curioni, X. Zhong, E. Koroleva, P. Skeldon, P. Thomson, M. Fowles, Discontinuities in the porous anodic film formed on AA2099-T8 aluminium alloy, Corros. Sci. 53 (2011) 4141-4151.

[9] D. Nickel, D. Dietrich, R. Morgenstern, I. Scharf, H. Podlesak, T. Lampke, Anodisation of aluminium alloys by micro-capillary technique as a tool for reliable, cost-efficient, and quick process parameter determination, Adv. Mater. Sci. Eng. (2016), Article ID 1374897, 12 page doi.org/10.1155/2016/1374897.

[10] S. Li, Y. Li, Y. Zhang, J. Liu, M. Yu, Effect of intermetallic phases on the anodic oxidation and corrosion of 5A06 aluminum alloy, Int. J. Miner. Metall. Mater. 22 (2015) 167-173.

[11] M.R. Kalantary, D.R. Gabe, D.H. Ross, Sealing of electrolytically formed porous films of aluminium by nickel fluoride process, Plat. Surf. Finish. 80 (1993) 52-56.

[12] Y. Zuo, P.-H. Zhao. J.-M. Zhao, The influences of sealing methods on corrosion behavior of anodized aluminum alloys in NaCl solutions, Surf. Coat. Technol. 166 (2003) 237-242.

[13] F. Mansfield, C. Chen, C.B. Breslin, D. Dull, Sealing of anodized aluminum alloys with rare earth metal salt solutions, J. Electrochem. Soc. 145 (1998) 2792-2798.

[14] M.R. Kalantary, D.R. Gabe, D.H. Ross, A model for the mechanism of nickel fluoride cold sealing of anodized aluminium, J. Appl. Electrochem. 22 (1992) 268-276.

[15] Naiping Hu, Xuecheng Dong, Xueying He, James F. Browning, Dale W. Schaefer, Effect of sealing on the morphology of anodized aluminum oxide, Corros. Sci. 97 (2015) 17-24.

[16] V.R. Capelossi, M. Poelman, I. Recloux, R.P.B. Hernandez, H.G. de Melo, M.G. Olivier, Corrosion protection of clad 2024 aluminum alloy anodized in tartaric-sulfuric acid bath and protected with hybrid sol–gel coating, Electrochim. Acta 124 (2014) 69-79.

[17] M. García-Rubio, M.P. de Lara, P. Ocón, S. Diekhoff, M. Beneke, A. Lavía, I. García, Effect of postreatment on the corrosion behaviour of tartaric–sulphuric anodic films, Electrochim. Acta, 54 (2009) 4789-4800.

[18] G.S. Frankel, R.L. McCreery, Inhibition of Al alloy corrosion by chromates, The Electrochemical Society Interface, Winter (2001) 34-38.

[19] M. Kendig, S. Jeanjaquet, R. Addison, J. Waldrop, Role of hexavalent chromium in the inhibition of corrosion of aluminium alloys, Surf. Coat. Technol. 140 (2001) 58-66.

[20] DEFSTAN 03-24/5. Chromic acid anodizing of aluminium and aluminium alloys, UK Ministry of Defence Specification (2008).

[21] D. Elabar, A Němcová, T. Hashimoto, P. Skeldon, G.E. Thompson, Effect of sulphate impurity in chromic acid anodizing of aluminium, Corros. Sci. 100 (2015) 377-385.

[22] D. Elabar, T. Hashimoto, J. Qi, P. Skeldon, G.E. Thompson, Effect of low levels of sulphate on the current density and film morphology during anodizing of aluminium in chromic acid, Electrochim. Acta 196 (2016) 206-212.

[23] R.G. Buchheit, R.P. Grant, P F. Hlava, B. McKenzie, G.L. Zender, Local dissolution phenomena associated with S phase (Al_2CuMg) particles in aluminum alloy 2024-T3, J. Electrochem. Soc. 144 (1997) 2621-2628.

[24] G.S. Chen, M. Gao, R.P. Wei, Microconstituent-induced pitting corrosion in aluminum alloy 2024-T3, Corros. 52 (1996) 8-15.

[25] A.E. Hughes, C. MacRae, N. Wilson, A. Torpy, T.H. Muster, A.M. Glenn, Sheet AA2024-T3: a new investigation of microstructure and composition, Surf. Interface Anal. 42 (2010) 334-338.

[26] A. Boag, A.E. Hughes, N.C. Wilson, A. Torpy, C.M. MacRae, A.M. Glenn, T. H. Muster, How complex is the microstructure of AA2024-T3?, Corros. Sci. 51 (2009) 1565-1568.

[27] P. Campestrini, E.P.M. van Westing, H.W. van Rooijen, J.H.W. de Wit, Relation between microstructural aspects of AA2024 and its corrosion behaviour investigated using AFM scanning potential technique, Corros. Sci. 42 (2000) 1853-1861.

[28] G.C. Wood, J.P. O'Sullivan, The anodizing of aluminium in sulphate solutions, Electrochim. Acta 15 (1970) 1865-1870.

[29] G.E. Thompson, R.C. Furneaux, G.C. Wood, Electron microscopy of ion beam thinned porous anodic films formed on aluminium, Corros. Sci. 18 (1978) 481-498.

[30] S. Ono, S. Yamashita, N. Masuko, Changes in thickness and degree of anion incorporation of anodic alumina films, in: Proceedings of the Second International Symposium on Aluminium Surface Science and Technology, Manchester, U.K., Benelux Metallurgie, 2000, p. 163-168.

[31] F. Zhou, A. K. Mohamed Al-Zenati, A. Baron-Wiecheć, M. Curioni, S. J. Garcia-Vergara, H. Habazaki, P. Skeldon, G. E. Thompson, Volume expansion factor and growth

efficiency of anodic alumina formed in sulphuric acid, J. Electrochem. Soc. 158 (2011) C202-C214.

[32] I. Mínguez-Bacho, S. Rodríguez-López, A. Climent, D. Fichou, M. Vázquez, M. Hernández-Vélez, Influence of sulfur incorporation into nanoporous anodic alumina on the volume expansion and self-ordering degree, J. Phys. Chem. C 119 (2015) 27392-27400.

[33] E. Jerrod, Houser, R. Kurt, Hebert, The role of viscous flow of oxide in the growth of self-ordered porous anodic alumina films, Nat. Mater. 8 (2009) 415-420.

[34] L. Iglesias-Rubianes, P. Skeldon, G.E. Thompson, H. Habazaki, K. Shimizu, Influence of current density in anodizing of an Al-W alloy, Corros. Sci. 43 (2001) 2217-2227.

[35] W.J. Stepniowski, M. Norek, M. Michalska-Domanska, A. Bombalska, A. Nowak-Stepniowska, M. Kwasny, Z. Boja, Fabrication of anodic aluminium oxide with incorporated chromate ions, Appl. Surf. Sci. 259 (2012) 324-330.

[36] J. Lambert, C. Guthmann, C. Ortega, M. Saint-Jean, Permanent polarization and charge injection in thin anodic alumina layers studied by electrostatic force microscopy, J. Appl. Phys. 91 (2002) 9161-9169.

[37] Ömer Özgür Çapraz, Pranav Shrotriya, Peter Skeldon, George E. Thompson, Kurt R. Hebert, Role of oxide stress in the initial growth of self-organized porous aluminium oxide, Electrochim. Acta 167 (2015) 404-411.

[38] A.C. Harness, L. Young, Can. J. Chem., High resistance anodic oxide films on aluminium, 44 (1966) 2409-2413.

[39] S. DeWit, K. Thornton, Model for anodic film growth on aluminum with coupled bulk transport and interfacial reactions, Langmuir 30 (2014) 5314-5324.

[40] Y. Oka , T. Takahashi, K. Okada, S. Iwai, Structural analysis of anodic alumina films, J. Non-cryst. Sol. 30 (1979) 349-357.

[41] R. Dupree, I. Farnan, A.J. Forty, S. El-Mashri, L. Bottyan, A MAS NMR study of the structure of amorphous aluminum films, J. Phys. 46 (1985) C8-113- C8-C117.

[42] J. Robinson, G.E. Thompson, Toward a structural model of anodic alumina, Proceedings of the Seventh International Symposium on Oxide Films on Metals and Alloys. Eds. K.R. Hebert and G.E. Thompson. The Electrochemical Society, Pennington NJ, Proceedings vol. 94-25 (1994) pp 1-10.

[43] I. Farnan, R. Dupree, A.J. Forty, Y.S. Jeong, G.E. Thompson, G.C. Wood, Structural information about amorphous anodic alumina from ^{27}Al MAS NMR, Philos. Mag. Lett. 59 (1989) 189-195.

[44] J. Oh, C.V. Thompson, The role of electric field in pore formation during aluminium anodization, Electrochim. Acta 56 (2011) 4044-4051.

[45] Omer O Capraz, Pranav Shrotriya. Peter Skeldon, George Thompson, Kurt Hebert,

Factors controlling stress generation during the initial growth of porous anodic aluminum oxide, Electrochim. Acta 159 (2015) 16-22.

[46] X. Zhou, G.E. Thompson, M.A.Paez, P. Skeldon, H. Habazaki, K. Shimizu, G.C. Wood, Morphological development of oxygen bubbles in anodic alumina, J. Electrochem. Soc. 147 (2000) 1747 -1750.

[47] G.E. Thompson, P. Skeldon. G.C. Wood, X. Zhou, U. Kreissig, E. Wieser, H. Habazaki, K. Shimizu, ERDA, RBS and TEM study of barrier film formation on Al-4.5 at.% Mg-0.05 at.% Cu alloy, Surf. Interface Anal. 27 (1999) 57-62.

[48] H. Habazaki, K. Takahiro, S. Yamaguchi, K. Shimizu, P. Skeldon, G.E. Thompson, G.C. Wood, Interfacial enrichment of iron during anodic oxidation of sputter-deposited Al-4 at.% Fe alloy, J. Electrochem. Soc. 146, (1999) 2502-2507.

[49] A.C. Crossland, G.E. Thompson, C.J.E. Smith, H. Habazaki, K. Shimizu, P. Skeldon, Formation of manganese-rich layers during anodizing of Al-Mn alloys, Corros. Sci. 41 (1999) 2053-2069.

[50] I. Pires, L. Quintino, C.M. Rangel, G.E. Thompson, P Skeldon, X. Zhou, Influence of pre-treatment on the surface condition of 2024-T3 aluminium alloy, Trans. Inst. Met. Finish. 78 (2000) 179-185.

[51] W.D. Mackintosh, F. Brown, H.H. Plattner, Mobility of metallic foreign atoms during the anodic oxidation of aluminium, J. Electrochem. Soc. 121 (1974) 1281-1286.

[52] F. Brown, W.D. Mackintosh, The use of Rutherford backscattering to study the behavior of ion-implanted atoms during anodic oxidation of aluminum: Ar, Kr, Xe, K, Rb, Cs, Cl, Br, and I, J. Electrochem. Soc. 120 (1973) 1096-1102.

[53] C. Cherki, J. Siejka, Study by nuclear microanalysis and O18 tracer techniques of the oxygen transport processes and the growth laws for porous anodic oxide layers on aluminium, J. Electrochem.Soc. 120 (1973) 784-791.

Figure captions

Figure 1. Current density–time curves for anodizing of aluminium at 100 V in chromic acid electrolytes of different SO_4^{2-} contents at 313 K. (a) SO_4^{2-} added as H_2SO_4. (b) SO_4^{2-} added as Na_2SO_4. LSCA and HSCA denote chromic acid electrolytes prepared from different sources of CrO_3 with no deliberate additions of SO_4^{2-}; the electrolytes contained ≤1.5 and 38 ppm SO_4^{2-}, respectively.

Figure 2. Scanning electron micrographs (secondary electrons) of cross sections of aluminium anodized at 100 V for 600 s in a chromic acid electrolyte containing 3000 ppm SO_4^{2-} at 313 K. (a) General view of the film in a cross-section cut with a diamond knife. (b) Detail of the pore morphology at a region of film fracture.

Figure 3. Bright field transmission electron micrographs of cross-sections of aluminium layers deposited by magnetron sputtering on electropolished aluminium, with an Al-W nanolayer deposited beneath the aluminium layer. (a) Before anodizing. (b) After anodizing at 100 V in a chromic acid electrolyte containing 900 ppm SO_4^{2-} (added as Na_2SO_4) at 313 K; anodizing was terminated when the tungsten nanolayer was incorporated into the barrier region of the porous film. Arrows in (a) and (b) indicate the location of the Al-W layer. (c) Detail of the barrier region. The vertical striations of light appearance in the barrier region are created by chatter during sectioning with the diamond knife.

Figure 4. Current density–time curves for anodizing of (a) aluminium and (b) AA 2024-T3 alloy using the Bengough-Stuart process (stepped voltage to a final value of 50 V) in LSCA

(≤1.5 SO_4^{2-}), HSCA (38 ppm SO_4^{2-}) and an electrolyte containing 1500 ppm SO_4^{2-} (added as Na_2SO_4) at 313 K.

Figure 5. Scanning electron micrographs (secondary electrons) of cross sections of aluminium anodized using the Bengough-Stuart process (stepped voltage to a final value of 50 V) in (a) LSCA ¯(≤1.5 SO_4^2), (b) HSCA (38 ppm SO_4^{2-}) and (c) an electrolyte containing 1500 ppm SO_4^{2-} (added as Na_2SO_4) at 313 K. (d) Detail of the pore morphology at a region of film fracture in the film of (c).

Figure 6. Scanning electron micrographs (backscattered electrons) of cross sections of AA 2024-T3 alloy anodized using the Bengough-Stuart process (stepped voltage to a final value of 50 V) in in (a) LSCA ¯(≤1.5 SO_4^2), (b) HSCA (38 ppm SO_4^{2-}) and (c) an electrolyte containing 1500 ppm SO_4^{2-} (added as Na_2SO_4) at 313 K.

Figure 7. Scanning electron micrographs (secondary electrons) of aluminium (a,b) and AA 2024-T3 alloy (c,d) anodized using the Bengough-Stuart process (stepped voltage to a final value of 50 V) in (a,c) LSCA (≤1.5 SO_4^{2-}) and (b,d) HSCA (38 ppm SO_4^{2-}) at 313 K. The films were stripped from the substrate by immersion in chromic/phosphoric acid.

Figure 8. Optical micrographs of the AA 2024-T3 alloy following anodizing using the Bengough-Stuart process (stepped voltage to a final value of 50 V) in (a) LSCA (≤1.5 SO_4^{2-}) and (b) HSCA (38 ppm SO_4^{2-}) at 313 K., and subsequent immersion for 15 days in naturally aerated 3.5 wt% NaCl solution at room temperature (~293 K). Insets show regions at increased magnification. (c,d) Scanning electron micrographs (secondary electrons) of the

respective specimens; (e,f) cross-sections at regions of localized film degradation on the respective specimens.

Table 1. S:Al atomic ratios determined by EDX point analyses at different depths in film cross-sections. The films were formed at either 100 V (Al 3000 ppm SO_4^{-2}) or by the Bengough-Stuart process (AA 2024-T3 1500 ppm SO_4^{2-} and Al-38 ppm SO_4^{2-} (HSCA)). The values at each depth were measured at three points at different regions of the cross-section. The average and standard deviation of the results are given.

Al-3000 ppm SO_4^{2-}		AA 2024 1500 ppm SO_4^{2-}		Al-38 ppm (HSCA)	
Depth in film	S:Al atomic ratio	Depth in film	S:Al atomic ratio	Depth in film	S:Al atomic ratio
(nm)		(nm)		(nm)	
200	0.050±0.005	200	0.035±0.005	200	0.012±0.001
750	0.040±0.003	750	0.026±0.004	700	0.003±0.004
1200	0.023±0.004	1550	0.027±0.005	1600	0.005±0.001
1700	0.023±0.003	2300	0.027±0.011	2200	no S detected
		2900	0.026±0.002		

Table 2. Charges densities passed during anodizing aluminium and AA 2024-T3 alloy.

	Anodizing condition	≤1.5 ppm (LSCA)	38 ppm (HSCA)	1500 ppm
		($C\ cm^{-2}$)		
Al	100 V/600 s	2.25±0.09	1.75±0.05	3.03±0.18
Al	B-S/2400 s	8.77±0.08	8.54±0.17	14.64±0.51
AA 2024	B-S/2400 s	17.63±0.1.62	12.69±1.09	12.11±0.07

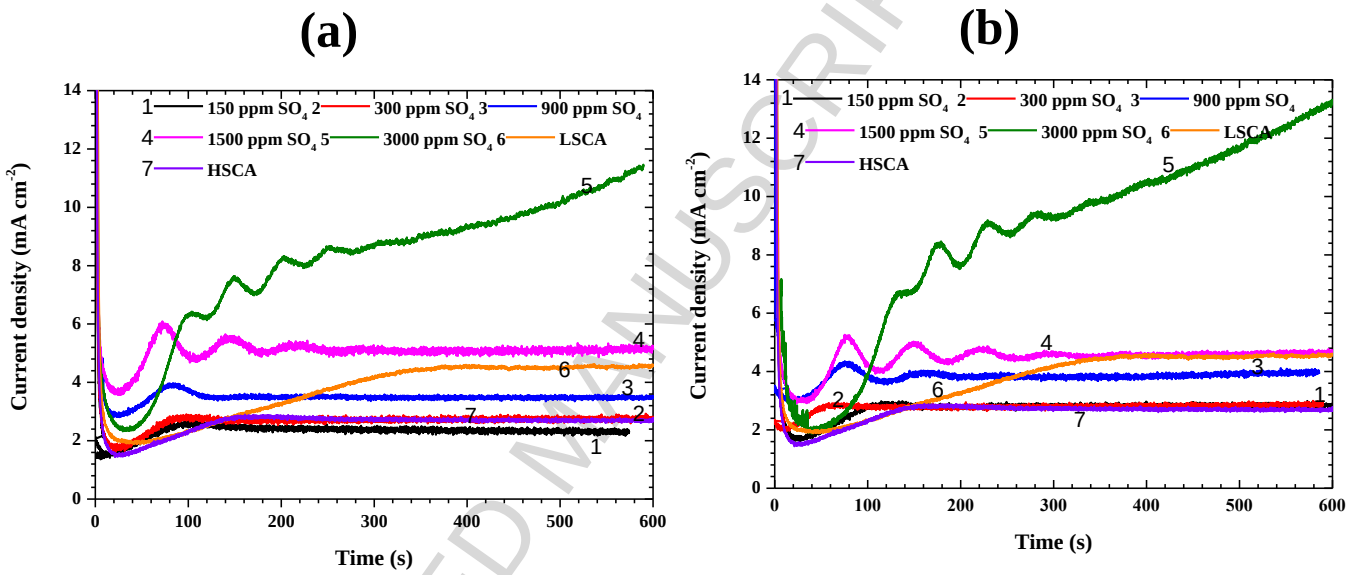

Figure 1

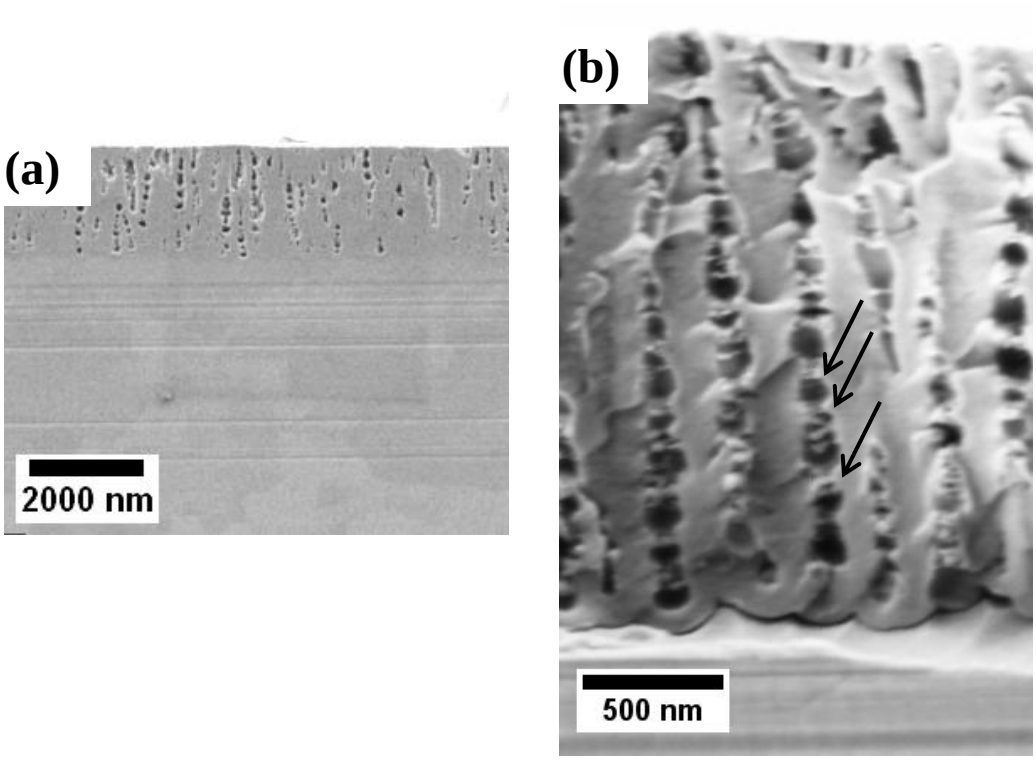

Figure 2

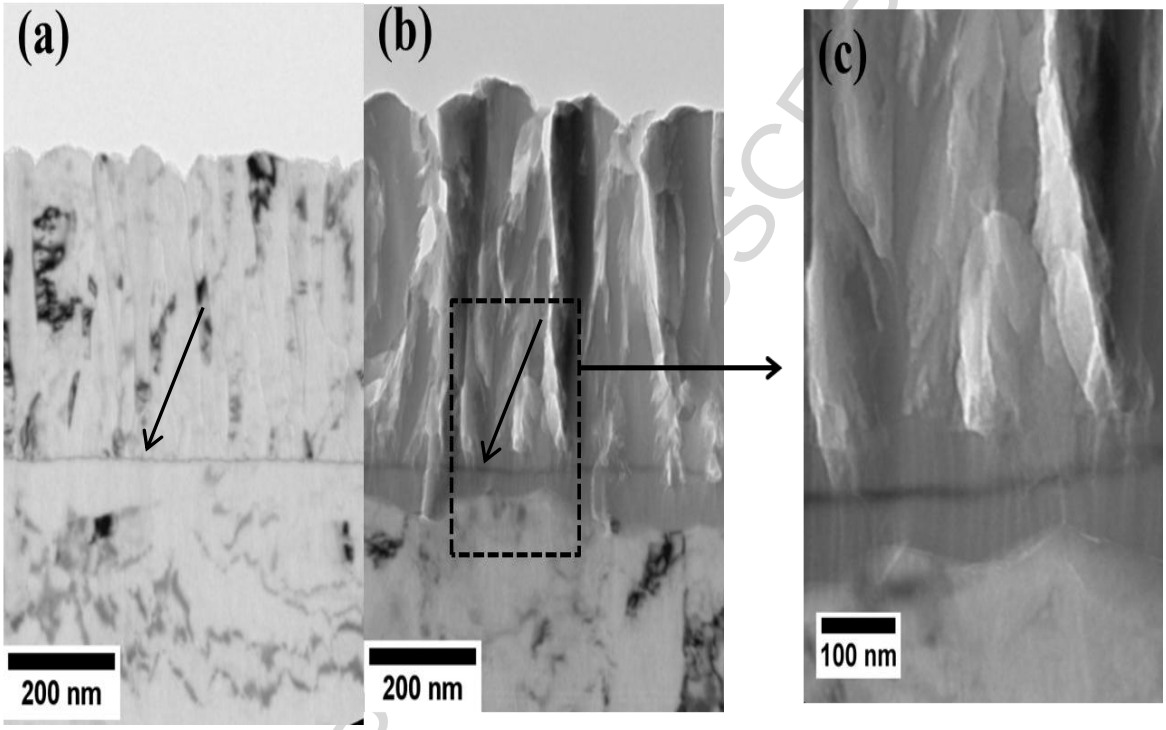

Figure 3

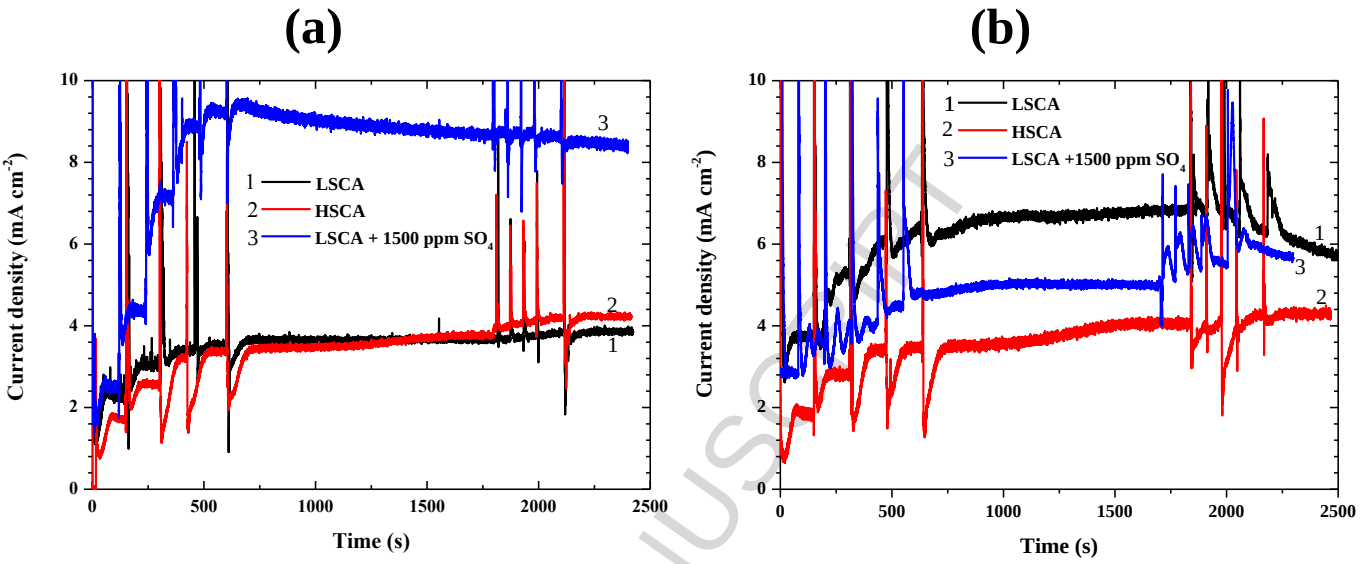

Figure 4

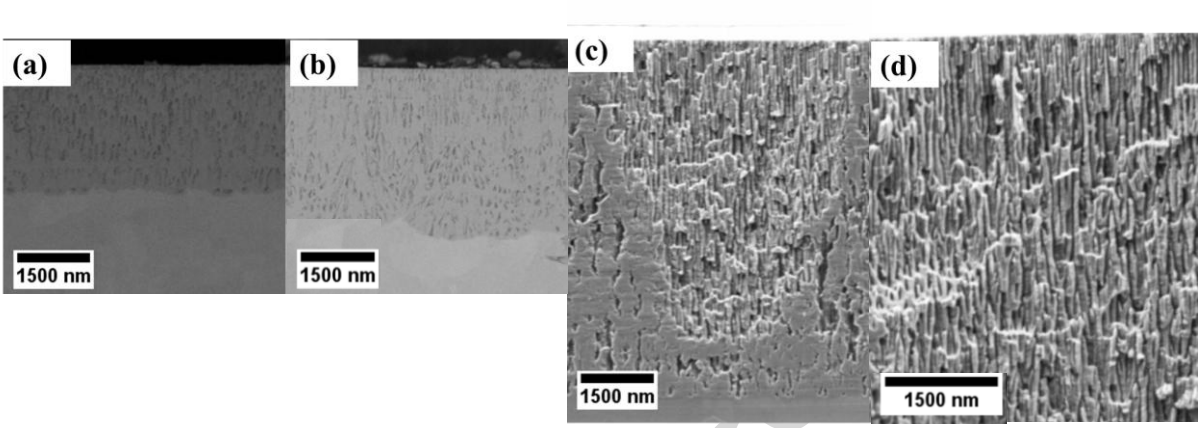

Figure 5

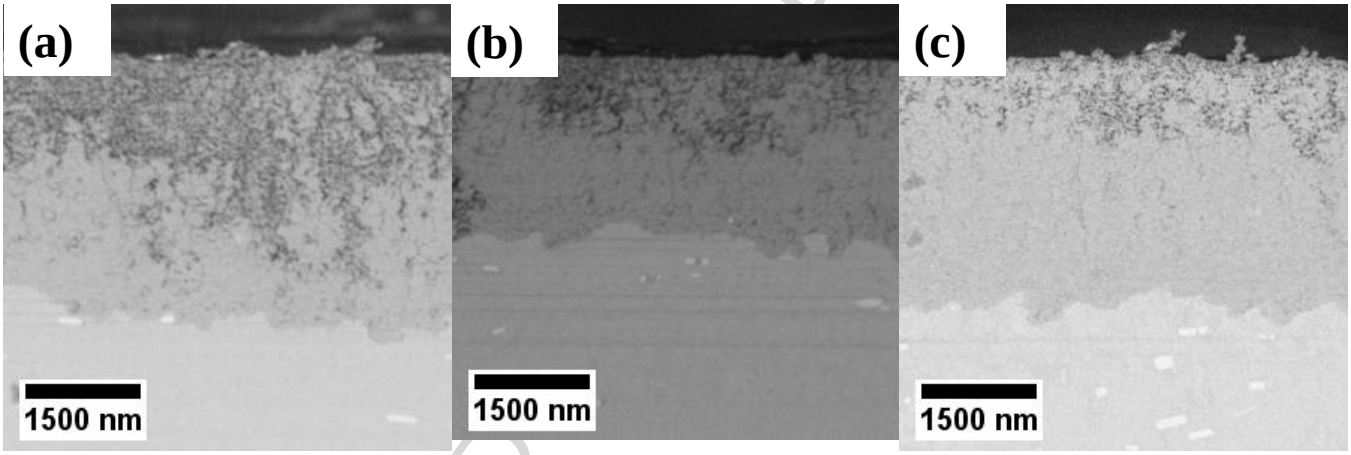

Figure 6

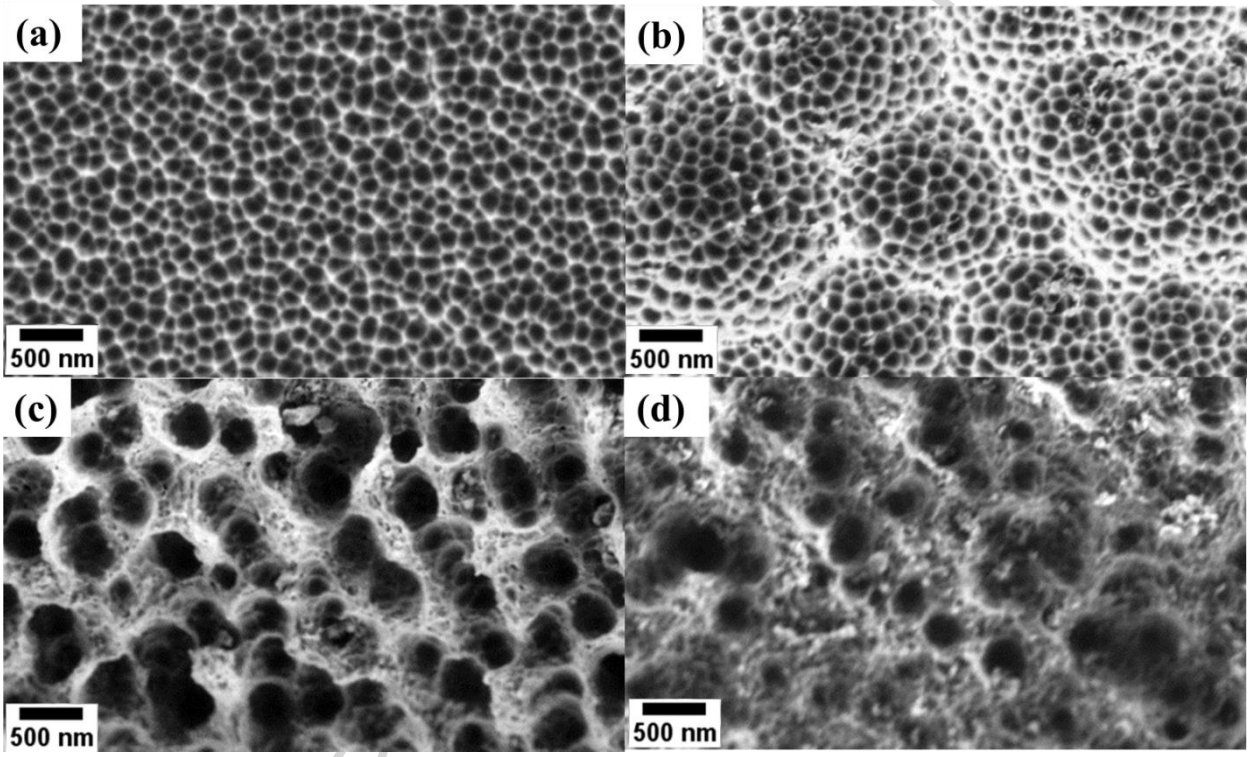

Figure 7

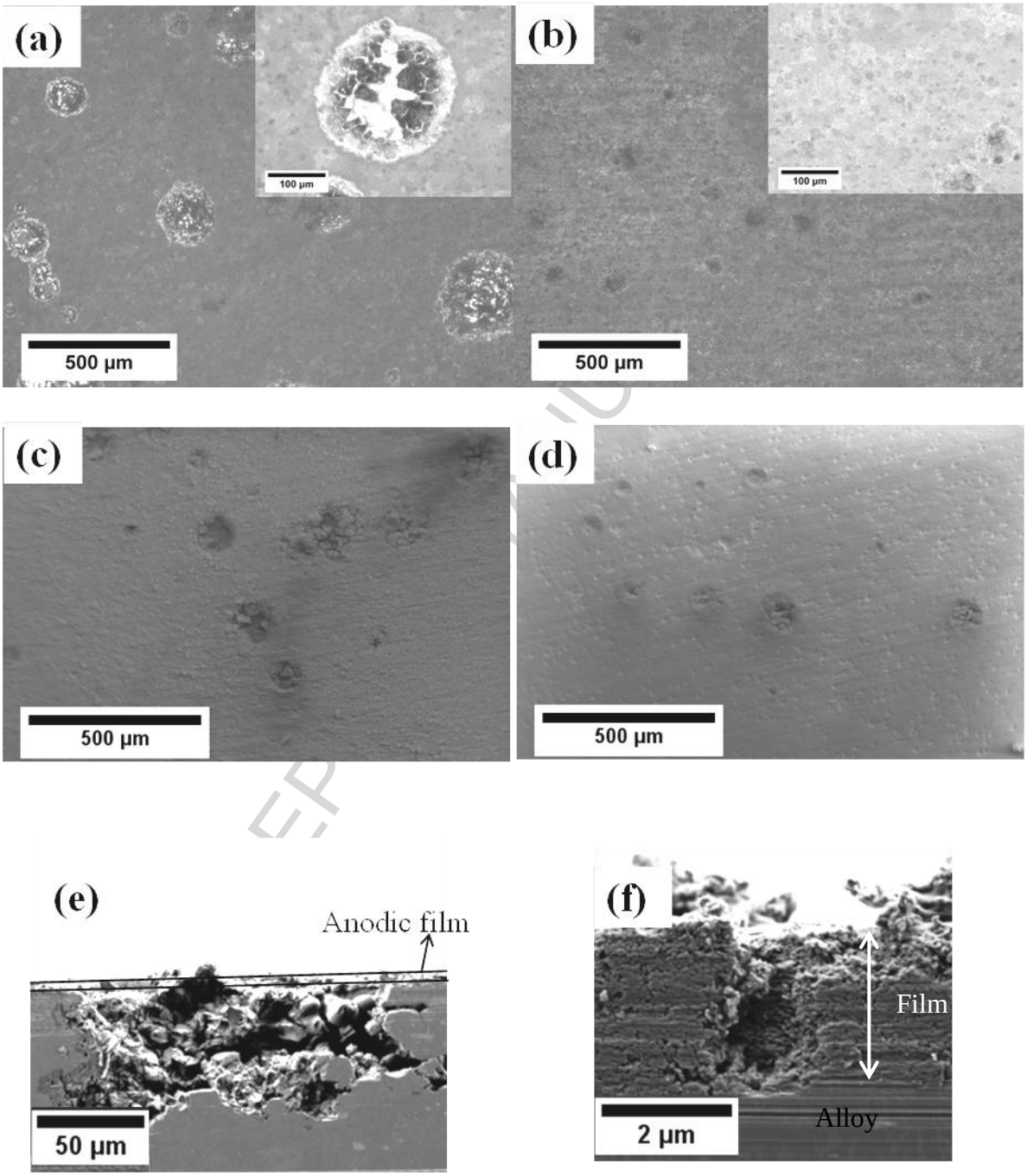

Figure 8

Highlights

- Film growth rate is affected by SO_4^{2-} impurity in chromic acid anodizing.
- SO_4^{2-} affects the film morphology and film composition.
- Effects depend on substrate composition, film morphology and oxygen generation.
- Unstable pore diameter occurs at high levels of SO_4^{2-} impurity.
- SO_4^{2-} impurity influences the corrosion protection provided by the anodic film.